Correlations between magnetic properties and bond formation in Rh-MgO(001)

Christopher WM Castleton[1,2], Somkiat Nokbin[1,3] and Kersti Hermansson[1]

[1]*Materials Chemistry, The Ångström Laboratory, Box 538, SE-751 21 Uppsala, Sweden*
[2]*Department of Physics and Measurement Technology, Linköping University, SE-581 83 Linköping, Sweden*
[3]*Laboratory for Computational and Applied Chemistry, Department of Chemistry, Kasetsart University, Bangkok 10900, Thailand*

Abstract

We present the results of first principles calculations for the magnetism of Rh adlayers on MgO (001), at three different adsorption sites and three different coverages, corresponding to 1, 1/2 and 1/8 monolayers. Finite magnetization is found in all cases except that of 1 Rh monolayer above the oxygen site, which is also the most stable. We examine how the magnetization changes as a function of the Rh-surface distance and relate this to changes in the real space charge density and in the density of states (DOS) as the Rh adlayer interacts with the surface. We find that increasing either the Rh-Rh interaction strength or the Rh-surface interaction strength leads to reduced magnetization, while increasing the former drives a crossover from localized (atomic) to itinerant magnetism. Neither the magnetic transition itself, nor the localized-to-itinerant magnetism crossover, is found to be directly related to the formation of Rh-surface bonds. From a practical point of view, we predict that magnetism in the Rh-MgO(001) system is most likely to be found experimentally at reduced coverages and at low temperatures.

1. Introduction

The study of magnetism in transition metals has a very long history. Most of the transition metals have a finite moment for the isolated atom, but magnetism in the three-dimensional (3D) bulk materials is very rare. Indeed, only four of the metals are magnetic and they are all from the first (3d) transition metal elements, with Fe, Co and Ni being ferromagnets and Mn an antiferromagnet. All the other 3d and all of the 4d and 5d transition metal atoms loose their magnetism when they bond together to form the bulk metals. However, in recent years there has been a great deal of interest in the possibility of forcing some of them to remain magnetic by reducing the dimensionality below that of the bulk metal. The interest is both fundamental and in the context of possible technological applications in spintronics and in magnetic data storage and retrieval. It has largely centred on the search for ferromagnetism in elements from the upper half of the second (4d) and third (5d) transition metal series. In this paper we will focus on one of the more commonly studied examples, Rh.

Rh has been shown to display a rich variety of magnetic behaviour as a function of dimensionality. Starting from *0D systems*: atomic Rh has the electronic configuration $4d^8 5s^1$, leading to a ground-state magnetic moment of 3 μ_B according to Hund's rules. 0D Rh_n ($n=9 \Rightarrow 34$) nano-clusters have been studied experimentally by Cox et al. [1,2], who found moments of $0.4 \Rightarrow 0.8$ μ_B for clusters with $n \leq 20$, dropping to $0.0 \Rightarrow 0.2$ μ_B above this size. Various theoretical studies [3-10] predict a rich variety of magnetic properties, with non-magnetic, ferromagnetic and antiferromagnetic ground states of $0 \Rightarrow 2$ μ_B all appearing for different values of n. In addition to this, 0D islands of Rh grown on Ag substrates have also been predicted to be magnetic [11].

Increasing to *1D systems*, Rh chains grown along the <010> and <110> directions on the (001) surface of Ag have been predicted to be magnetic [11,12]. However, experimental growth of such systems has been found to be very hard to control, so they are currently of limited interest technologically.

More interesting is the possibility of keeping Rh magnetic in *2D systems* [13]. The most obvious 2D system is actually the surface of bulk Rh crystals, and spin-dependent photoemission [14] does indeed find a weak magnetization of 0.2 μ_B, in agreement with theoretical predictions [15]. More "strictly" 2D systems have also been studied, in the form of Rh thin films and monolayers (MLs) grown on a variety of substrates. Here, most of the systems examined have been Rh adlayers on noble metal substrates. Theoretical predictions have suggested that single Rh MLs will be magnetic on Ag (111) [16,17] and (001) [13,16,18-24], Au (111) [16] and (001) [13,16,23,25], Ni (111) [26] and Cu (001) [16,27-29] but non-magnetic on Ag (110) [16], Au (110) [16], Cu (110) [16] and Cu (111) [16]. In the magnetic cases, the moments are predicted to

decrease rapidly with increasing numbers of Rh layers, usually becoming very weak by film thicknesses of just 2 ML [26,30]. Unfortunately, all attempts to experimentally demonstrate the presence of a magnetic moment in such a system have failed [31-33]. The explanation seems to be that layer-by-layer growth is too difficult to obtain on these substrates, due to problems with lattice constant mismatch, interdiffusion and alloying [29,34]. Theoretical work shows that this should indeed destroy the anticipated magnetism [18,24,35].

The obvious alternative is to study MLs grown on *non*-metallic substrates. So far one such transition metal system has been found to be magnetic: Ru grown on C(0001) [36,37]. Experimental studies of Rh MLs on non-metallic substrates have (to our knowledge) yet to be reported, but theoretical predictions suggest that Rh should remain magnetic on C(0001) [37-39], albeit weakly. One further non-metallic substrate has been considered theoretically: MgO. Experimentally, MgO(001) is used frequently as a substrate for metallic thin film growth (see references [40-48], for example). As for the 3d metals, Li and Freeman [40] have studied magnetism theoretically in the Fe/MgO(001) system. They predicted a very large moment of $3.07\mu_B$ for Fe, almost the same as that they found for the free Fe ML ($3.10\ \mu_B$). Moreover, 2 ML of Fe on MgO(001) has also been predicted to be magnetic, with magnetic moments of 2.85 and $2.96\ \mu_B$ for the first and second ML, respectively [40]. Theoretical calculations for various 4d transition metals on MgO(001) have also been reported. Using full-potential linearized augmented-plane-wave (FLAPW) periodic calculations (see Ref. [49] for details) Wu and Freeman [42] found that 1 ML Ru and Rh films on MgO(001) remain magnetic, with moments of $1.95\ \mu_B$ and $1.21\ \mu_B$, respectively. However, Nokbin et al. [50] recently examined the Rh/MgO system using a planewave basis and the projector augmented wave (PAW) method and found finite moments only for adsorption at the metastable Mg and "hollow" sites (see later); at the more stable O site the adsorbed ML was found to be non-magnetic, contradicting the results of Wu and Freeman.

In the present paper we will resolve the discrepancy between these two theoretical predictions. We will examine how magnetism in the Rh/MgO(001) system is switched on and off, and how this depends upon the chemical bonding both within the adsorbed layer (the Rh-Rh interactions) and between the ad-layer and the substrate (Rh-surface interactions). In so doing we hope to give a better guide to experimentalists looking for magnetism in 4d transition metal systems, as well as a clearer understanding of the relationship between magnetism and bonding in *metal on metal oxide systems* in general. We will do this by relating the evolution of the magnetic moment to details of the electronic structure as a function of the adlayer-substrate distance and by discussing how this relates to the so-called Stoner criterion. The electronic structure of the Rh/MgO system itself is also interesting in other chemical and technological contexts, most

notably in heterogeneous catalysis. The functionality of Rh/MgO catalysts has therefore been studied intensively experimentally; see for example Ref. [51,52].

Magnetic transitions are usually characterized and discussed in terms of the Stoner Criterion. [53,54] This states that a system may have a non-zero magnetic moment if the exchange energy gained by becoming magnetic exceeds the kinetic energy penalty: hence if $I \bullet N(\varepsilon_F) > 1$, where I is the Stoner parameter (see below), and $N(\varepsilon_F)$ is the density of states (DOS) at the Fermi level, ε_F. The density of states value $N(\varepsilon_F)$ is inversely proportional to the bandwidth, and hence to the kinetic energy. The exchange energy is quantified by the Stoner parameter, I, which becomes large when the spatial confinement of the electrons at ε_F is large. Magnetism is thus favoured by small bandwidths (large $N(\varepsilon_F)$) and by strong spatial confinement of the electronic wavefunctions (large I). The dependence of these on changes in the bonding are easy to track via plots of the DOS and of the charge and spin densities and derivatives of them. In principle, I can be evaluated from the calculated wavefunction, but here we only need a framework for discussion, so we will consider only rough changes in I as evidenced by changes in charge density and related properties. The more important contributions come from $N(\varepsilon_F)$, however, since I is dominated by the atomic region rather than its surroundings.

The alternative way to view the Stoner criterion is to say that magnetism is favoured when the states near ε_F (in this case the 4d states of the Rh) become more atomic-like. The extreme cases for Rh are thus the free atom (very sharp peaks in the DOS) and the bulk (fairly flat DOS at ε_F). An important distinction should be drawn here, between atomic-like (i.e. localized) and "itinerant" (delocalized) magnetism. In the former case, the magnetic electrons are completely localized in atomic-like states, flat in momentum space, and do not contribute to electrical and thermal transport. In this case, only integer multiples of the single electron magnetic moment ($1\mu_B$) can occur. In the latter case, the magnetized electrons, while still fairly localized, belong none-the-less to a band with significant bandwidth. They are thus at least partially delocalized and do contribute to the transport properties. In this case only the total magnetic moment for the whole sample is an integer, so the moment per atom or per primitive unit cell may be any rational number from zero up to the free atom moment. In the present study we will find a crossover between the two regimes, as well as crossovers between magnetic and non-magnetic regimes.

2. Method and system geometry

All calculations were performed using periodic planewave density functional theory (DFT) with the Vienna Ab initio Simulation Package, VASP [55,56]. The PAW method [57,58] was used, as implemented in VASP, with exchange and correlation described using the "PW91" generalized

gradient approximation (GGA) [59]. Spin-polarized calculations were performed with a planewave cut-off energy of 500 eV in all cases. (For comments on convergence, see below.) The valence electronic configurations of the atomic species employed were Rh($4p^6$,$5s^1$,$4d^8$), Mg($2p^6$,$3s^2$) and O($2s^2$,$2p^4$). Integration over k-points was done using Gaussian smearing with a Gaussian width equal to 0.1 eV (except where otherwise noted) and the Brillouin zone was sampled over 6x6x6 and 6x6x1 Monkhorst-Pack (MP) [60] meshes for bulk and surface calculations, respectively. The structures were optimized until all the forces on unconstrained atoms were less than 0.01 eV/Å. In this paper, we are concerned mainly with the magnetic properties of the Rh/MgO(001) system. We report magnetic moments defined by

$$\mu = \int_{-\infty}^{\varepsilon_F} [N_\uparrow(\varepsilon) - N_\downarrow(\varepsilon)] d\varepsilon$$

where $N_\uparrow(\varepsilon)$ and $N_\downarrow(\varepsilon)$ are the majority and minority spin components, sometimes referred to as the α and β components, respectively. The moments are thus given for the complete supercell, although we will also report projected moments on individual atoms. The atom projected moments were obtained using Wigner-Seitz projection [62] onto spheres of radii of 1.402, 1.058 and 0.820 Å around the Rh, Mg and O atoms, respectively.

Three different coverages (1/8, 1/2 and 1 ML) at three different sites (on top of O, Mg and the hollow) were explored for the Rh/MgO(001) system, as shown in **Fig 1.** The periodic models used were as follows: A single Rh layer was placed on one side of the MgO oxide slab and a vacuum gap of 15 Å was used (see below.) In addition, calculations for isolated Rh layers and for Rh bulk and the Rh atom were performed (see below).

For 1/2 and 1 ML coverages, the calculation cell consisted of 8 MgO layers plus a vacuum gap along *z* and a 1x1 crystallographic unit cell in the *x* and *y* directions and. For the lowest coverage (1/8 ML), a 2x2 crystallographic unit cell in the *x* and *y* directions was used, with 4 MgO layers along *z*. For all systems, all atoms were allowed to fully relax in all directions under the condition that the orthogonal unit cell was kept fixed at the optimized GGA bulk lattice parameter of 4.25 Å in the *x* and *y* directions. (The experimental cell parameter of bulk MgO is 4.21 Å. Incidentally, our optimized bulk cell parameter for fcc bulk Rh is 3.85 Å and the experimental value is 3.80 Å [61]).

To ensure that the planewave cutoff and k-point sampling had been properly converged for the various bulk, surface and adatom systems, several test calculations were performed. We found that increasing the k-point grids from 6x6x1/6x6x6 to 8x8x1/8x8x8 for the surface/bulk calculations altered the calculated total energies by O(0.01) eV/O(0.00001) eV. This was tested for clean bulk MgO, and for the Rh/MgO system with 1 and 1/2 ML Rh at the O site.) The calculated magnetic moments remained the same to O(0.01) μ_B. Increasing the planewave cutoff

from 500 eV to 600 eV resulting in changes of O(0.0001) eV in the total energy of the free atom but for all other cases it made changes of O(0.1) eV in the total energy. This is large, but we are only interested in differences between total energies, and these are much better: the adsorption energies at the O and hollow sites with 1 ML and 1/2 ML coverage are converged to O(0.01) eV, while the energy differences between the O and hollow sites are converged to O(0.001) eV. The magnetic moments are all converged to O(0.001) μ_B or better with a 500 eV planewave cutoff. Regarding the models themselves, increasing the number of MgO layers in the slab from 4 to 5 for 1/8 ML altered the Rh adsorption energy by only O(0.001) eV at the O site. Increasing the vacuum gap from 15 to 20 Å alters the clean surface total energy by less than 0.001 eV, so adsorption energies etc should be still better converged. Indeed, reducing the vacuum gap to 10 Å only produces total energy errors of less than 0.01 eV (relative to a 20 Å gap), so results should be well converged even when the Rh atom is placed high above the surface.

3. Results and discussion

3.1. Magnetic properties of the Rh atom and Rh isolated layers

As reference systems, the isolated Rh atom and bulk Rh metal were studied, together with the three different isolated Rh MLs, corresponding to the three different coverages. These were all studied using the same potentials, plane-wave cutoff etc. as for the Rh/MgO systems. The DOS for bulk and atomic Rh and for the three isolated MLs are shown in **Fig 2**, while the magnetic moments obtained for the isolated MLs are listed in **Table 1**.

For *atomic Rh*, the expected magnetic moment is 3 μ_B, since the ground state configuration is $4d^8 5s^1$. 2 μ_B of the moment comes from the 4d shell and 1 μ_B from the 5s. Using the Gaussian width of 0.1 eV for the smearing – to maintain consistency with all our other results – we find calculated magnetizations of 1.97 μ_B and 1.96 μ_B in supercells of 10.0 and 20.0 Å, respectively. (This becomes 1.39 μ_B using the Wigner-Seitz projection, in agreement with the previous value of 1.38 μ_B from Moruzzi and Marcus [63].) The problem arises partly because the PAW potential used in this study has been generated to obtain accurate results for Rh in compounds and molecules, not for the free atom, so the smearing of 0.1 eV is sufficient to mix the 4d and 5s giving us an actual configuration of $4d^{8.5}5s^{0.5}$, instead of that expected. This gives contributions of 1.5 μ_B and 0.5 μ_B from the 4d and 5s shells, respectively – hence the 2 μ_B total obtained. In principle this can be corrected by fixing the occupancies of the Kohn-Sham orbitals to force the expected $4d^8 5s^1$ configuration. However, the energies obtained by this method are not very meaningful. Instead we can overcome the problem by reducing the smearing to 0.001 eV. This gives us the correct $4d^8 5s^1$ configuration, a magnetization of 3 μ_B and a total energy 0.222 eV

lower. However, for the purpose of consistency, we have used the Rh atom results calculated with a Gaussian width of 0.1 eV for the calculation of the adsorption energies (see later).

Bulk Rh is non-magnetic. The Rh-Rh bonding will, of course, make the 4d electrons less localized, reducing *I*. As seen in **Fig 2,** it also leads to a broad 4d band and hence to a low $N(\varepsilon_F)$. The Stoner criterion is thus not met and so there is no splitting between $N_\uparrow(\varepsilon)$ and $N_\downarrow(\varepsilon)$.

The isolated free Rh monolayers all consist of 2D square lattices with nearest-neighbour Rh-Rh distances of 8.50, 4.25 and 3.00 Å, corresponding to the 1/8, 1/2 and 1 ML systems, respectively. Calculations were done in supercells of the same dimensions as those used for the full Rh/MgO slab cases. As we go from 1/8 to 1/2 to 1 ML, the 4d band progressively widens as the nearest neighbour distance decreases, resulting in increased Rh-Rh interaction, and specifically d-d hybridization, within the layer. $N(\varepsilon_F)$ thus decreases in the order 1/8 ML > 1/2 ML > 1 ML, with the first value closely resembling the free atom and the last resembling bulk Rh. The Stoner criterion is clearly fulfilled for all of the isolated MLs, but more strongly for the 1/8 ML layer and less strongly for the 1 ML layer, as evidenced by the calculated total magnetic moments of 1.97, 1.69 and 1.57 μ_B/atom for the 1/8, 1/2 and 1 ML, respectively. (The latter figure is in good agreement with the previous calculations of Zhu et al.[25]) If the Wigner-Seitz projections described earlier are used this becomes 1.40, 1.40 and 1.46 μ_B/atom.

3.2. Magnetic properties of the Rh/MgO(001) interface

Table 1 also lists the total magnetic moments of the whole cell for the various Rh/MgO systems. **Table 2** lists the corresponding Wigner-Seitz-projected moments for the Rh atoms and for those surface-layer Mg and O atoms which lie closest to the adsorbed Rh atoms. The moments are shown at the optimal Rh-surface distances for the various cases, as listed. The main contribution to the magnetic moment is always from Rh, with small induced moments in the O atoms in the surface layer. The contribution of the Mg atoms is negligible. From our previous work [43] and [50] we know that the most stable adsorption site is the O site for all coverages, with the hollow and Mg sites being only metastable. For the 1 ML cases, the O, Mg and hollow sites have total magnetic moments (for the whole cell) of 0.00, 1.48 and 1.42 μ_B/Rh atom, respectively. For the 1/2 ML, all the systems are magnetic with moments of 1.00, 1.58 and 1.13 μ_B/Rh atom at the O, Mg and hollow adsorption sites, respectively. The magnetic moment for 1/8 ML at the O site is 1.00 μ_B/Rh atom. Hence the adsorption site dependence of the magnetic moments comes in the order O < hollow < Mg, independent of coverage. The magnetic moments at the O site increase in the order 1 ML < 1/2 ML < 1/8 ML. Qualitatively, the coverage (or Rh density) dependence of the magnetism in the adsorbed MLs is thus similar to that of isolated free Rh MLs, but it may be more informative to note that the magnetic moments have the opposite trend to the ML-

substrate interaction energies: the larger the interaction energy, the smaller the magnetic moment. This agrees well with findings in the literature (see, for example, Ref. [64]).

The only Rh/MgO case for which we do not get a magnetic moment is for 1 ML at the O site. This is confirmed by the plot in **Fig 3**, which shows the energy as a function of total magnetic moment, taken from a series of Fixed Spin Moment (FSM) calculations, [65,66] (Each calculation is performed by minimizing the total energy subject to the constraint that the total magnetic moment in the supercell is equal to a pre-determined values.) The curve is fairly linear, with a slope of approximately 0.05 eV/μ_B, and a ground state of $\leq$0.1 μ_B. (The figure does indicate that the energy is very flat for moments $\leq$0.2μ_B, but we believe this to be a numerical problem). The zero moment for 1 ML at the O site directly contradicts the results of Wu et al. [42], who found a magnetic moment of 1.21 μ_B. To see why, we show in **Fig 4** the magnetic moment as a function of Rh-surface distance d. The curves for the O site and for all the other sites and coverages were obtained by taking the relaxed atomic positions from the optimized Rh/MgO structure for the case in question, and then keeping all the positions within both the MgO slab and the Rh layer fixed and just rigidly moving the Rh layer relative to the MgO surface with no further relaxation. For all of the sites, and at all coverages, the Rh layer starts out with magnetic moments the same as those of the isolated layers when $d \approx 5$ Å. In most cases this starts to fall for $d \approx$ 2-3 Å, as the Rh layer starts to interact with the surface, before dropping to zero at some shorter distance. The details of the curves vary with adsorption site, indicating the sensitivity of the Rh magnetism to details of the environment around the adsorbed atom. They also vary strongly with coverage, indicating the sensitivity to the weakening of the intra-layer d-d hybridization – in effect, sensitivity to the dimensionality. However, in almost all cases, the optimal distance d_o occurs before the moment falls to zero. The exception is for 1 ML at the O site, where d_o = 2.10 Å, with the moment having fallen to zero between 2.20 and 2.15 Å. Wu and Freeman [42] obtained an optimal distance of d_o = 2.34 Å. On our plot this would result in a moment of ~1.4 μ_B, which is rather close to the moment they obtained. They chose to fix the lattice constant in the x and y directions to the experimental value (rather than the relaxed GGA one), which leads to a small unphysical strain in the x-y plane. This in turn will have adversely affected their relaxed bond lengths and angles by a small but possibly significant amount. Although it is not conclusive, we also find a more stable interface energy (0.95 eV versus 0.84 eV).

3.3. The relationship between bond formation and magnetism at the Rh/MgO(001) interface

Figs 5 to 9 illustrate the changes in the electronic, magnetic and bonding behaviour for various cases as a function of d. More specifically, the DOS, the Rh atom projected DOS, as well as the charge density, ρ, the charge density difference $\Delta\rho$ and the spin density $\sigma = \rho_\uparrow + \rho_\downarrow$, are plotted

as a function of d. The $\Delta\rho$ shown is the charge density ρ for the complete Rh/MgO system minus the sum of the charge densities for the isolated Rh layer (i.e. without the MgO slab) and the clean MgO slab (i.e. without the Rh layer), using the same atomic positions in the three calculations involved. In other words it shows the changes in ρ resulting from the interaction *between the layer and the slab*. It provides a neat way to view the real-space changes in the electronic structure resulting from the interactions and bonding between the systems.

3.3.1 1 ML Rh at the O site

Fig 5 shows the behaviour of the 1 ML Rh/MgO over the O site. For large d ($\geq$ 3.00 Å), the total DOS has two distinct peaks (although the Rh-projected DOS indicates more substructure). The strongest peak lies just below ε_F, leading to a large value for $N(\varepsilon_F)$. The $\Delta\rho$ maps show the electron redistribution in the Rh layer caused by the interaction with the oxide substrate and the redistribution is seen to be modest for largest d value (rightmost figure in the third row of **Fig 5**), suggesting that the Stoner parameter I is also large. We therefore expect $I \bullet N(\varepsilon_F)$ to be large, meeting the Stoner criterion: indeed we find a reasonably strong splitting between the spin up ($N_\uparrow$) and down ($N_\downarrow$) components of the Rh 4d levels and a finite magnetic moment of 1.55 μ_B, similar to that of the isolated Rh layer.

As the Rh layer is brought in from 4.78 Å to 2.25 Å above the surface, the electronic structure undergoes a qualitative change as the layer starts to interact with the surface, as seen in the DOS. At the same time the charge density in the oxide surface layer is rearranged, but seemingly in a gradual fashion, as evidenced by the $\Delta\rho$ maps. The σ maps show that a magnetic moment is induced on the surface oxygen atoms as d is decreased from 3.78 to 3.00 Å, leading to a slight rise in the magnetization, in agreement with **Fig 4**. The electron density is seen to decrease between the Rh and the surface O (see the $\Delta\rho$ maps), as well as in the region above the Rh atom, and is spread out in between the Rh, in the region above the surface Mg. Hence it appears that the "in-layer" Rh-Rh interaction (d-d hybridization) is actually enhanced by the Rh-surface interaction. This results in the Rh 4d electrons becoming gradually less localized (and hence the Stoner parameter I gradually smaller) as d is reduced. The 4d band in the DOS becomes broader, and the main peaks become weaker and move to lower energies, resulting in a much lower value of $N(\varepsilon_F)$.

However, what it at remarkable – at least at first glance - is that the qualitative changes in the electronic structure, as evidenced by the change in the Rh-projected DOS at d = 3.00 $\Rightarrow$ 2.25 Å, leave the Rh magnetization virtually unchanged. Instead, when the moment *does* disappear, it does so sharply at d = 2.25 $\Rightarrow$ 2.10 Å, even though there is almost no visible change in the DOS, ρ or $\Delta\rho$ here. In other words, it is not in itself the adhesion of the Rh to the surface that switches

off the magnetism. Certainly, the qualitative changes to the electronic structure at longer distances *do* reduce $I \bullet N(\varepsilon_F)$, and but they do not take it below 1. Instead it is a gradual transition, in which the value of $I \bullet N(\varepsilon_F)$ falls smoothly, finally dipping below 1 without any qualitative changes to the electronic structure taking place at all. In fact, this results in the magnetization vs *d* curve shown for the O site in figure 4a) being very close to the idealized Stoner criterion plots found in textbooks, with our *d* playing the role of (and presumably proportional to) $I \bullet N(\varepsilon_F)$.

3.3.2 1/2 and 1/8 ML Rh at the O site

Figures 6 and **7** show the DOS, projected DOS, $\Delta\rho$ and σ as a function of *d* for the cases of, respectively, 1/2 and 1/8 ML Rh over O. The total DOS, ρ, $\Delta\rho$ and σ are very similar to the 1 ML systems although the features are smaller due to the lower density of Rh. The Rh atoms themselves are further apart, so the Rh-Rh interactions are much smaller, leading to both higher localization (larger *I*) and narrower Rh projected DOS (larger $N(\varepsilon_F)$), and hence to stronger magnetic effects. Indeed, the projected DOS for the 1/8 ML case is very atomic-like, and the resulting magnetization should probably be an integer multiple of μ_B for all *d*. It is for $d < 3$ Å, but, unfortunately, we have convergence problems above this, as seen in Fig 4b. These are no doubt due to the same problem met with the free atom. We could in principle get around them by forcing the expected Kohn-Sham occupancies, but the results would not be very informative – certainly not if we wanted to know where the 2 μ_B to 3 μ_B transition occurs. Worse, here we cannot get around the problems by simply relying on a smaller smearing, as that would also make the description of the slab worse. Instead, we have examined the results of a range of different k-point integration methods. (The k-point grid itself is still well converged using 6x6x1[‡].) We have tried both Gaussian and Methfessel-Paxton (order 1 and 2) [67] smearing with widths of 0.1 and 0.005 eV, as well as Fermi smearing and the tetrahedron method with and without Blöchl corrections [68]. The values plotted in Fig. 4 use Gaussian smearing with a width of 0.1 eV, while the error bars indicate the highest and lowest values obtained with the other schemes: they essentially vary from 2 to 3 μ_B depending upon whether the Rh layer or the MgO slab is badly treated. Nevertheless, the results are mostly consistent with an integer value of 2 μ_B, which is itself consistent with the values obtained for the isolated layer and for the free Rh atom.

As a function of increasing Rh density (hence, increasing d-d hybridization) we thus see a crossover between itinerant and localized (atomic) magnetism. The 1/8 ML moment itself changes from 2 (or perhaps 3) μ_B to 1 μ_B at about $d = 2.8$ Å, accompanied this time by changes in $\Delta\rho$. We cannot find the change from 1 to 0 μ_B, as it happens at such short distances that the results are difficult to converge numerically and not very meaningful physically. The results for

[‡] For example, for $d = 5$ Å the energy difference obtained between fixed magnetizations of 2 and 3 μ_B is 0.0927 for 6x6x1, 0.0911 eV for 8x8x1 and 0.0910 eV for 10x10x1, using Gaussian smearing with width = 0.005 eV.

the very small d values, given here and elsewhere, are reported to help examine the magnetic transitions in the Rh/MgO system, but the accuracy and physicality of these results are certainly much reduced compared to the results for, say, $d > 1.5$ Å.

For the 1/2 ML case, there is again a qualitative change in the charge density and bonding accompanying the magnetic transition. The DOS and projected DOS show distinct changes a little above the magnetic transition (around $d \approx 1.5$ Å) and a gradual decrease in $N(\varepsilon_F)$ at the transition itself. Meanwhile, $\Delta\rho$ shows the charge being pushed outwards to accumulate above the Rh atoms ($d = 0.75$ Å) in an area which shows charge depletion for larger d values. Hence the magnetic transition seems to be driven in this case by a gradual change in $N(\varepsilon_F)$ and a sudden change in I caused by the Rh crashing into the O atom below it. Meanwhile, the crossover from itinerant to localized magnetism is actually seen here as a function of d. Around the optimal distance ($d_o = 2.10$) and below we find atomic-like DOS and integer moments. For larger distances we find non-integer moments. The accompanying changes in ρ, $\Delta\rho$ and σ are again gradual, so, like the 1ML magnetic transition, the itinerant/localized magnetism crossover is not directly linked to bonding changes.

3.3.3 1/2 and 1 ML Rh at the Mg and Hollow sites

The total and projected DOS, $\Delta\rho$ and σ for 1 ML at the two metastable sites are shown in Figs 8 and 9. The total and projected DOS and σ are actually strikingly similar to the DOS for 1 ML Rh at the O site (above the transition), and show a similar evolution with d. The Rh 4d electrons become gradually more spread out and the DOS broadens slightly, weakening the magnetic moment. The $\Delta\rho$, on the other hand is very different. Comparing $\Delta\rho$ for all three sites as d is reduced it always shows a depletion of charge between Rh and O, and an accumulation of charge between Rh and Mg. For the O site, this leads to accumulation between the Rh atoms and depletion above and below. For the Mg site, it leads to depletion between the Rh atoms and accumulation below and above. For the hollow site it leads to a twisted, diagonal pattern, with Rh atoms separated by regions of both accumulation and depletion. Hence, the d-d hybridization is enhanced for the O site (decreasing both $N(\varepsilon_F)$ and I), but is reduced at the other two. This appears to be the reason why Rh is non-magnetic at d_0 at the O site, but remains magnetic at the other two.

For both sites, as d is reduced below 2 Å the Rh and Mg atoms start to overlap more strongly, an induced moment appears for a while on the neighbouring Mg atoms. This leads to the increases in magnetization at $d \approx 1.5$ Å and 1.25 Å for the hollow and Mg sites, respectively, as seen in **Fig 4a.** Finally, for the hollow site only weak changes are seen at the magnetic transition, (mostly in $\Delta\rho$ for $d \geq 2.5$ Å) but for the Mg site a very distinct change is observed in $\Delta\rho$ and DOS. Electron density is suddenly transferred from the Rh and neighbouring Mg atoms to Mg

and O atoms in the second layer of the MgO slab, and this sudden reduction in the localization kills off the magnetic moment.

4. Conclusion

We previously [43,50] showed that the most stable site for Rh adsorption on MgO(001) is the O site and found that it is nonmagnetic at 1 ML coverage, in contradiction to an earlier study. Here we have confirmed that it is indeed non-magnetic at 1ML coverage, but that it is magnetic at 1/2 and 1/8 ML coverages, and at the metastable Mg and hollow sites. The energy difference between magnetic and non-magnetic ground states is 0.1 eV for 1/2 ML at the O site; the others are similar. We have then studied the dependence of the Rh magnetic moment upon the chemical interactions within the layer and between the layer and the surface by examining the DOS, projected DOS, ρ, $\Delta\rho$ and σ as a function of coverage, site and surface-adlayer distance d.

As the Rh layer is brought towards the MgO slab, they start to interact. At some point the shape of the DOS, particularly the Rh-projected DOS, changes qualitatively, illustrating changes in the Rh-Rh and Rh-surface interactions. $\Delta\rho$ is seen to change more gradually as a function of d; thus some bonding changes appear to be more easily detected in the DOS curves. As d shrinks, the Rh projected DOS gets gradually wider and $N(\varepsilon_F)$ gradually smaller. For Rh adsorbed at the O site, the charge becomes more spread out into the region between the Rh atoms, thus becoming less localized, so that the Stoner parameter I shrinks. At some point the Stoner criterion ceases to be fulfilled and the magnetism switches off. For the 1/2 and 1/8 ML O site cases, as well as for the 1 ML Mg site case, this happens at the same point as the qualitative changes in the DOS, and hence in the bonding. For the 1 ML O and hollow site cases, on the other hand, it does not. In other words, the presence of a magnetic moment and the formation or enhancement of the intra-layer or layer-slab bonding are not directly connected.

In addition to the magnetic transition and its variations with coverage and site, we have also observed a crossover from localized (integer moment) to delocalized (fractional moment) magnetism as a function of coverage. The lower the coverage the smaller the d-d hybridization, and hence the more localized the magnetism.

As a function of Rh-Rh and Rh-surface interaction strengths we thus find regions of both localized and itinerant magnetism as well as non-magnetic regions. This is illustrated in **Fig 10**, which shows the magnetic moment plotted against estimates of the Rh-Rh and Rh-surface interaction strengths. The Rh-Rh interaction is estimated by the formation energies of the isolated layers and the Rh-surface interaction strength by the adsorption energies. Moments are plotted for the isolated layers and for all three adsorption sites, at all coverages calculated, but only at the optimal distances. The trend is that increasing either the Rh-Rh interaction (d-d

hybridization) or the Rh-surface interaction leads to reduced magnetic moments, and increasing the d-d hybridization drives the system from localized to itinerant magnetism. Having studied here only one 4d metal on one surface it is difficult to know whether the phase diagram shown in **Fig 10** is generic, but the present example at least suggests a strategy. When searching for magnetic 4d and 5d thin films and monolayers one might want to examine systems in which the adlayer and the surface interact only weakly and which preferably have low coverage in order to keep the average d-d hybridization low. In the case of Rh on the MgO (100) surface it is certainly necessary to go to coverages below 1 ML. The critical coverage lies between 1/2 and 1 ML, but where exactly we cannot say; this is perhaps an important question for future computational work.

Further computational work is also needed to determine how important the structural ordering of the Rh adlayer is for the presence of magnetism at low coverages. We are not aware of any experiments preparing or characterizing submonolayer films of Rh on MgO, but island growth is preferred for several other metal/MgO systems. [69,70,71] For a specific coverage the key to finding magnetism is having only weak d-d hybridization, so island size is a potential issue. Large islands will probably be non-magnetic, while small islands or homogeneously distributed adatoms are likely to remain magnetic. These could probably be ordered or disordered, or even link to form networks, as long as the Rh-Rh coordination remains low. One of these latter situations is the most promising for an experimental demonstration of magnetism in Rh/MgO systems. For instance, recent calculations [72] have predicted that growth of a disordered but homogeneous film is favoured over island growth in the presence of surface defects, a situation which can probably be engineered during substrate preparation. Low temperature experiments are likely to be needed in order to stabilize both structure and magnetism.

Acknowledgements

This work was supported by the Swedish Foundation for International Cooperation in Research and Higher Education, (STINT) and the Swedish Research Council (VR). S.N. wishes to thank the Thailand Research Fund (TRF) for a Royal Golden Jubilee Ph.D. fellowship (3.C.KU/43/A.2). The authors also acknowledge the use of the Ngorongoro computer system at the Department of Information Technology, Uppsala University and the Lenngren and Swegrid facilities run by the Swedish National Infrastructure for Computing. We would also like to thank Susanne Mirbt for helpful discussions.

References

[1] A. J. Cox, J. G. Louderback, L. A. Bloomfield, Phys. Rev. Lett. 71 (1993) 923.

[2] A. J. Cox, J. G. Louderback, S. E. Apsel, L. A. Bloomfield, Phys. Rev. B 49 (1994) 12295.

[3] C. Barreteau, R. Guirado-Lopez, D. Spanjaard, M. C. Desjonqueres, A. M. Oles, Phys. Rev. B 61 (2000) 7781.

[4] Z.-Q. Li, J.-Z. Yu, K. Ohno, Y. Kawazoe, Sci. Rep. Res. Inst. Tohoku Univ. Phys. Chem. Metall. 40 (1995) 297.

[5] J. Yang, K. Deng, C. xiao, K. Wang, Phys. Status Solidi B 195 (1996) 549.

[6] B. V. Reddy, S. N. Khanna, B. I. Dunlap, Phys. Rev. Lett. 70 (1993) 3323.

[7] K. Lee, Z. Phys. D: At., Mol. Clusters 40 (1997) 164.

[8] Y. Jinlong, F. Toigo, W. Kelin, Surf. Rev. Lett. 3 (1996) 323.

[9] V. Kumar, Y. Kawazoe, Eur. Phys. J. D 24 (2003) 81.

[10] B. V. Reddy, S. K. Nayak, S. N. Khanna, B. K. Rao, P. Jena, Phys. Rev. B 59 (1999) 5214.

[11] K. Wildberger, V. S. Stepanyuk, P. Lang, R. Zeller, P. H. Dederichs, Phys. Rev. Lett. 75 (1995) 509.

[12] D. I. Bazhanov, W. Hergert, V. S. Stepanyuk, A. A. Katsnelson, P. Rennert, K. Kokko, C. Demangeat, Phys. Rev. B 62 (2000) 6415.

[13] S. Blügel, Phys. Rev. Lett. 68 (1992) 851.

[14] S. C. Wu, K. Garrison, A. M. Begley, F. Jona, P. D. Johnson, Phys. Rev. B 49 (1994) 14081.

[15] J.-H. Cho, M. Scheffler, Phys. Rev. Lett. 78 (1997) 1299.

[16] L. M. Garcia-Cruz, R. Baquero, Rev. Mex. Fis. 49 (2003) 317.

[17] J. Redinger, S. Bluegel, R. Podloucky, Phys. Rev. B 51 (1995) 13852.

[18] I. Turek, J. Kudrnovsky, M. Sob, V. Drchal, P. Weinberger, Phys. Rev. Lett. 74 (1995) 2551.

[19] A. M. N. Niklasson, S. Mirbt, H. L. Skriver, B. Johansson, Phys. Rev. B 56 (1997) 3276.

[20] R. Wu, A. J. Freeman, Phys. Rev. B 45 (1992) 7222.

[21] S. Blügel, Solid State Commun. 84 (1992) 621.

[22] O. Eriksson, R. C. Albers, A. M. Boring, Phys. Rev. Lett. 66 (1991) 1350.

[23] B. Ujfalussy, L. Szunyogh, P. Weinberger, Phys. Rev. B 51 (1995) 12836.

[24] A. Mokrani, H. Dreysse, S. Bouarab, C. Demangeat, J. Magn. Magn. Mater. 113 (1992) 201.

[25] M. J. Zhu, D. M. Bylander, L. Kleinman, Phys. Rev. B 43 (1991) 4007.

[26] Z. V. Sljivancanin, F. R. Vukajlovic, J. Phys.: Condens. Matter 10 (1998) 8679.

[27] C. S. Chang, L. H. Cho, J. I. Lee, S. C. Hong, R. Wu, A. J. Freeman, J. Magn. Magn. Mater. 177-181 (1998) 1255.

[28] A. E. Garcia, V. Gonzalez-Robles, R. Baquero, Phys. Rev. B 59 (1999) 9392.

[29] A. B. Hayden, T. Valla, D. P. Woodruff, J. Phys.: Condens. Matter 7 (1995) 9475.

[30] S. Blügel, Phys. Rev. B 51 (1995) 2025.

[31] I. Chado, F. Scheurer, J. P. Bucher, Phys. Rev. B 64 (2001) 094410/1.

[32] G. A. Mulhollan, R. L. Fink, J. L. Erskine, Phys. Rev. B 44 (1991) 2393.

[33] C. Liu, S. D. Bader, Phys. Rev. B 44 (1991) 12062.

[34] C. Demangeat, S. Bouarab, H. Dreysse, Int. J. Mod. Phys. B 7 (1993) 488.

[35] W. Hergert, P. Rennert, C. Demangeat, H. Dreysse, Surf. Rev. Lett. 2 (1995) 203.

[36] R. Pfandzelter, G. Steierl, C. Rau, Phys. Rev. Lett. 74 (1995) 3467.

[37] L. Chen, R. Wu, N. Kioussis, J. R. Blanco, J. Appl. Phys. 81 (1997) 4161.

[38] P. Kruger, A. Rakotomahevitra, G. Moraitis, J. C. Parlebas, C. Demangeat, Physica B 237-238 (1997) 278.

[39] P. Kruger, J. C. Parlebas, G. Moraitis, C. Demangeat, Computational Materials Science 10 (1998) 265.

[40] C. Li, A. J. Freeman, Phys. Rev. B 43 (1991) 780.

[41] Y. Y. Huang, C. Liu, G. P. Felcher, Phys. Rev. B 47 (1993) 183.

[42] R. Wu, A. J. Freeman, Phys. Rev. B 51 (1995) 5408.

[43] S. Nokbin, J. Limtrakul, K. Hermansson, Surf. Sci. 566-568 (2004) 977.

[44] C. Martinez Boubeta, C. Clavero, J. M. Garcia-Martin, G. Armelles, A. Cebollada, L. Balcells, J. L. Menendez, F. Peiro, A. Cornet, M. F. Toney, Phys. Rev. B 71 (2005) 014407/1.

[45] F. Didier, J. Jupille, Surf. Sci. 307-309 (1994) 587.

[46] G. Renaud, A. Barbier, O. Robach, Phys. Rev. B 60 (1999) 5872.

[47] O. Robach, G. Renaud, A. Barbier, Phys. Rev. B 60 (1999) 5858.

[48] M. P. Delplancke, P. Delcambe, L. Binst, M. Jardinier-Offergeld, F. Bouillon, Thin Solid Films 143 (1986) 43.

[49] P. Blaha, K. Schwarz, P. Sorantin, S. B. Trickey, Comput. Phys. Commun. 59 (1990) 399.

[50] S. Nokbin, C.W.M. Castleton, J. Limtrakul, K. Hermansson, (to be published).

[51] F. Solymosi, J. Cserenyi, L. Ovari, J. Catal. 171 (1997) 476.

[52] H. Y. Wang, E. Ruckenstein, J. Catal. 186 (1999) 181.

[53] M. M. Sigalas, D. A. Papaconstantopoulos, Phys. Rev. B 50 (1994) 7255.

[54] G. Fabricius, A. M. Llois, H. Dreysse, Phys. Rev. B 48 (1993) 6665.

[55] G. Kresse, J. Hafner, Phys. Rev. B 47 (1993) 558.

[56] G. Kresse, J. Furthmueller, Phys. Rev. B 54 (1996) 11169.

[57] P. E. Blöchl, Phys. Rev. B 50 (1994) 17953.

[58] G. Kresse, D. Joubert, Phys. Rev. B 59 (1999) 1758.

[59] J. P. Perdew, J. A. Chevary, S. H. Vosko, K. A. Jackson, M. R. Pederson, D. J. Singh, C. Fiolhais, Phys. Rev. B 46 (1992) 6671.

[60] H. J. Monkhorst, J. D. Pack, Phys. Rev. B 13 (1976) 5188.

[61] H. P. Singh, Acta Crystallogr., Sect. A: Found. Crystallogr. 24 (1968) 469.

[62] A. Eichler, J. Hafner, J. Furthmueller, G. Kresse, Surf. Sci. 346 (1996) 300.

[63] V. L. Moruzzi, P. M. Marcus, Phys. Rev. B 39 (1989) 471.

[64] A. J. Freeman, R. Q. Wu, J. Magn. Magn. Mater. 100 (1991) 497.

[65] A.R. Williams, V.L. Moruzzi, J. Kübler and K. Schwarz Bull. Am. Phys. Soc 29 (1984) 278 (1984).

[66] K. Schwarz and P. Mohn J. Phys. F: Met. Phys 14 (1984) L129 (1984).

[67] M. Methfessel, A. T. Paxton, Phys. Rev. B 40 (1989) 3616.

[68] P. E. Blöchl, O. Jepsen, O. K. Andersen, Phys. Rev. B 49 (1994) 16223.

[69] J. H. Larsen, J. T. Ranney, D. E. Starr, J. E. Musgrove and C. T. Campbell Phys. Rev. B 63 (1996) 195410.

[70] C.R. Henry Surf. Sci. Rep. 31 (1998) 231.

[71] J. T. Ranney, D. E. Starr, J. E. Musgrove, D. J. Bald and C. T. Campbell, Faraday Discuss. 114 (1999) 195.

[72] D. Fuks, Y.F. Zhukovskii, E.A. Kotomin and D.E. Ellis Surf. Sci. 600 (2006) L99.

Table 1. Total magnetization (in μ_B per Rh atom) for the Rh/MgO(001) system for different Rh coverages at the optimized Rh-surface distances. Values for isolated Rh layers corresponding to the three coverages are also given. The magnetization for the isolated gas-phase Rh atom is 1.959 μ_B (see text).

	Total magnetization per Rh atom and optimized Rh-surface distance (in parenthesis)		
	1/8 ML	**1/2 ML**	**1 ML**
Isolated Rh layer	1.966[b]	1.685[a], 1.703[b]	1.566[a], 1.610[b]
Rh/MgO			
Rh above O	0.999 (2.00 Å)	0.999 (2.10 Å)	0.002 (2.10 Å)
Rh above Mg		1.575 (2.77 Å)	1.480 (2.93 Å)
Rh above hollow		1.134 (1.96 Å)	1.423 (2.52 Å)

[a]Calculated using the 1x1 crystallographic cell and 8 MgO layers, as in Fig. 1a.

[b]Calculated using the 2x2 crystallographic cell and 4 MgO layers, as in Fig. 1c.

Table 2. Atom-projected spin magnetic moments (in μ_B) corresponding to the total magnetizations given in Table 1. The magnetic moments were calculated within standard Wigner-Seitz spheres with radii 1.402, 1.058 and 0.820 Å, respectively, for Rh, Mg and O. The magnetic moments listed for Mg and O in the table refer to those top-layer atoms which are either nearest or next-nearest neighbours of the Rh atom. All other atoms have magnetic moments close to zero.

	Atom-projected spin magnetic moments (in μ_B)								
	1/8 ML			**1/2 ML**			**1 ML**		
	Rh	**Mg_{surf}**	**O_{surf}**	**Rh**	**Mg_{surf}**	**O_{surf}**	**Rh**	**Mg_{surf}**	**O_{surf}**
Isolated Rh layer	1.398 [b]			1.398,[a] 1.408[b]			1.463,[a] 1.487[b]		
Rh/MgO									
Rh above O	0.882	-0.001	0.049	0.933	-0.002	0.003	0.000	0.000	0.000
Rh above Mg				1.310	-0.001	0.018	1.357	-0.001	0.027
Rh above hollow				0.998	-0.003	0.034	1.286	-0.002	0.049

[a]Calculated using the 1x1 crystallographic cell and 8 MgO layers, as in Fig. 1a.

[b]Calculated using the 2x2 crystallographic cell and 4 MgO layers, as in Fig. 1c.

Figure captions

Fig 1. (a) The surface coverage definitions for the Rh/MgO(001) systems, as seen "from above" (i.e. along *z*). The crosses mark the adsorption sites of Rh (always O in the example in the figure). (b) The supercell shown consists of 1x1 crystallographic unit cells in the *x* and *y* directions, and the coverage illustrated is 1 ML. (c) The supercell shown consists of 1x1 crystallographic unit cells in the *x* and *y* directions, and the coverage illustrated is 1/2 ML. (d) The supercell shown consists of 2x2 crystallographic unit cells in the *x* and *y* directions, and the coverage illustrated is 1/8 ML. The lines denoted P1, P2 and P3 define the sections used for the various electron density and spin density plots.

Fig 2. DOS for bulk Rh and isolated Rh layers (exactly corresponding to the various, slighly buckled, optimized adlayer geometries resulting from the Rh/MgO(001) calculations). The solid and dashed lines represent the $N_{\uparrow}(\varepsilon)$ and $N_{\downarrow}(\varepsilon)$ (majority and minority) spin components, respectively.

Fig 3 The relative energy of the Rh/MgO(001) system (1 ML on O) as a function of the system magnetization, calculated for a Rh-O distance of 2.10 Å.

Fig 4 Total magnetization of the Rh/MgO system as a function of the interlayer distance between the Rh overlayer and the surface for (a) different adsorption sites of 1ML coverage and (b) different coverages at the O site. See section 3.3.2 for a detailed discussion of the error bars.

Fig 5. Two energy-related and three electron-density related properties for Rh/MgO(001) plotted as a function of the Rh-O distance, for adsorption of 1 ML of Rh on top of O. Starting from the optimized geometry, the distance between the Rh layer and the oxide slab was varied, keeping their respective geometries fixed. For the DOS and Rh projected DOS, the majority and minority spin components are shown, in states/eV. The total electron density, the difference electron density, i.e. $\Delta\rho(\mathbf{r}) = \rho(\text{Rh/MgO}) - [\rho(\text{Rh-layer in the same geometry}) + [\rho(\text{MgO-slab in the same geometry})]$ and the spin density, $\sigma(\mathbf{r})$, are shown as contour plots, where solid and dashed contour lines represented electron excess and electron loss, respectively. The contour lines start at ± 0.0005 e/a.u.^{3}, increasing by a factor of $10^{0.2}$ for every contour line, i.e. they are at 0.0034, 0.0053, 0.0085, 0.0134, 0.0213, 0.0338, 0.0535, 0.0848, 0.1344, 0.2130, 0.3377, 0.5352, 0.8483, 1.3445, ... e/Å^3, and correspondingly for the negative contours.

Fig 6. The same types of plots as in Fig. 5, but for 1/2 ML Rh coverage on the O sites.

Fig 7. The same types of plots as in Fig. 5, but for 1/8 ML Rh coverage on the O sites.

Fig 8. The same types of plots as in Fig. 5, but for 1 ML Rh coverage on the Mg sites.

Fig 9. The same types of plots as in Fig. 5, but for 1 ML coverage of Rh on the "hollow" sites.

Fig 10. Schematic magnetic phase diagram for the Rh/MgO(001) system. This shows our calculated regions of localized and itinerant magnetism and paramagetism, plotted as a function of the Rh-Rh and Rh-surface interaction strengths (see text for details). The diagram includes results from the calculations for all the different coverages and interaction sites at the optimal layer-slab distance for each case.

Figure(s)

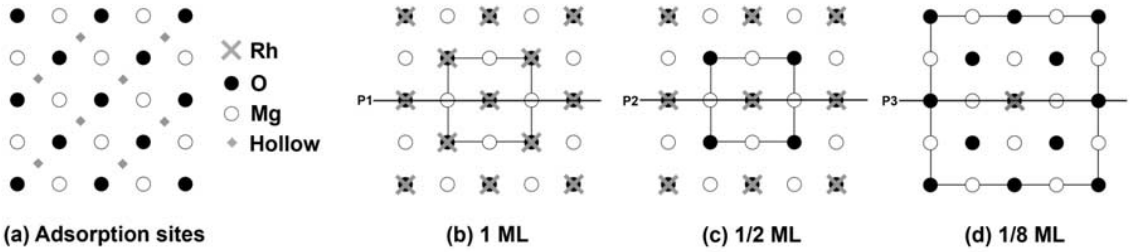

Fig 1

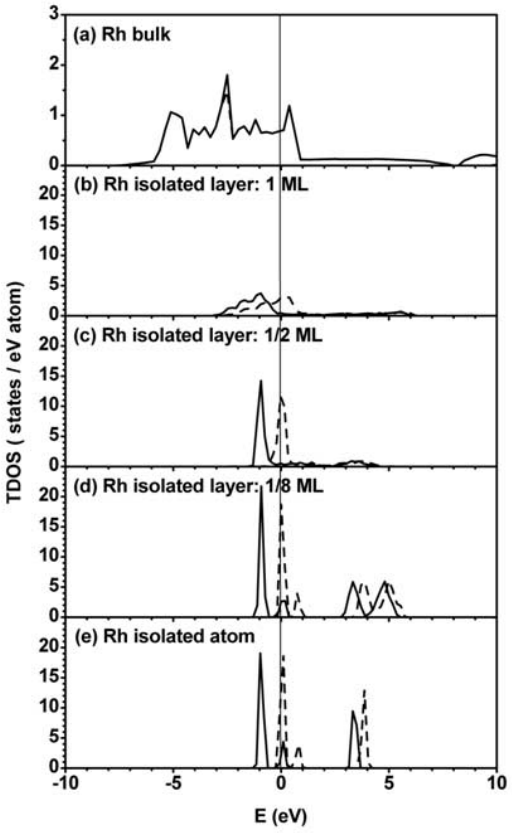
(a) Rh bulk
(b) Rh isolated layer: 1 ML
(c) Rh isolated layer: 1/2 ML
(d) Rh isolated layer: 1/8 ML
(e) Rh isolated atom
TDOS (states / eV atom)
E (eV)

Fig 2

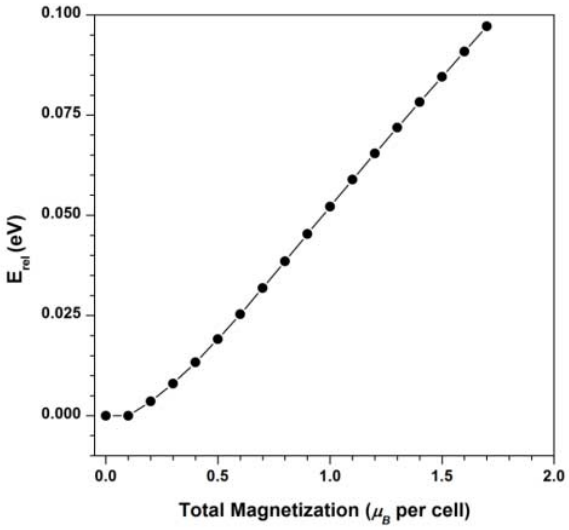
0.100
0.075
0.050
0.025
0.000
E_rel (eV)
0.0
0.5
1.0
1.5
2.0
Total Magnetization (μ_B per cell)

Fig 3

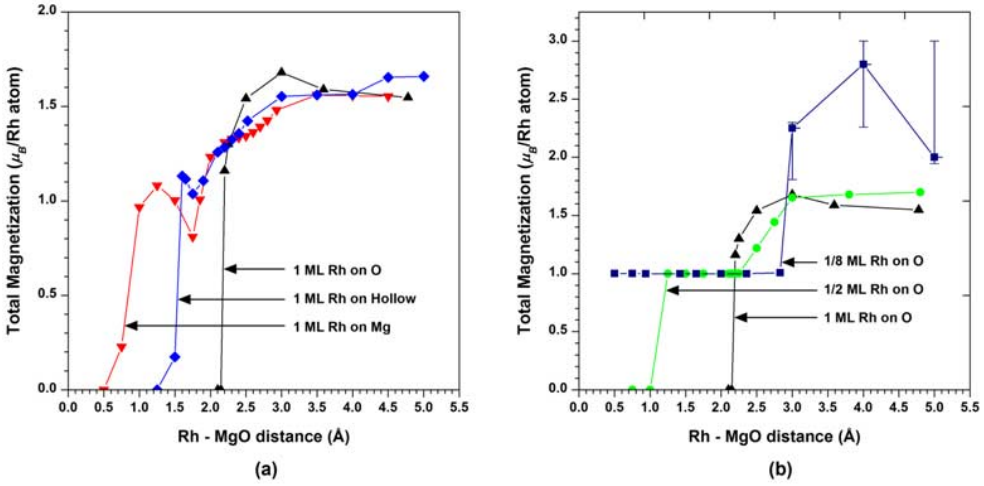
Total Magnetization (μ_B/Rh atom)
Rh - MgO distance (Å)
1 ML Rh on O
1 ML Rh on Hollow
1 ML Rh on Mg
(a)
Total Magnetization (μ_B/Rh atom)
Rh - MgO distance (Å)
1/8 ML Rh on O
1/2 ML Rh on O
1 ML Rh on O
(b)

Fig 4

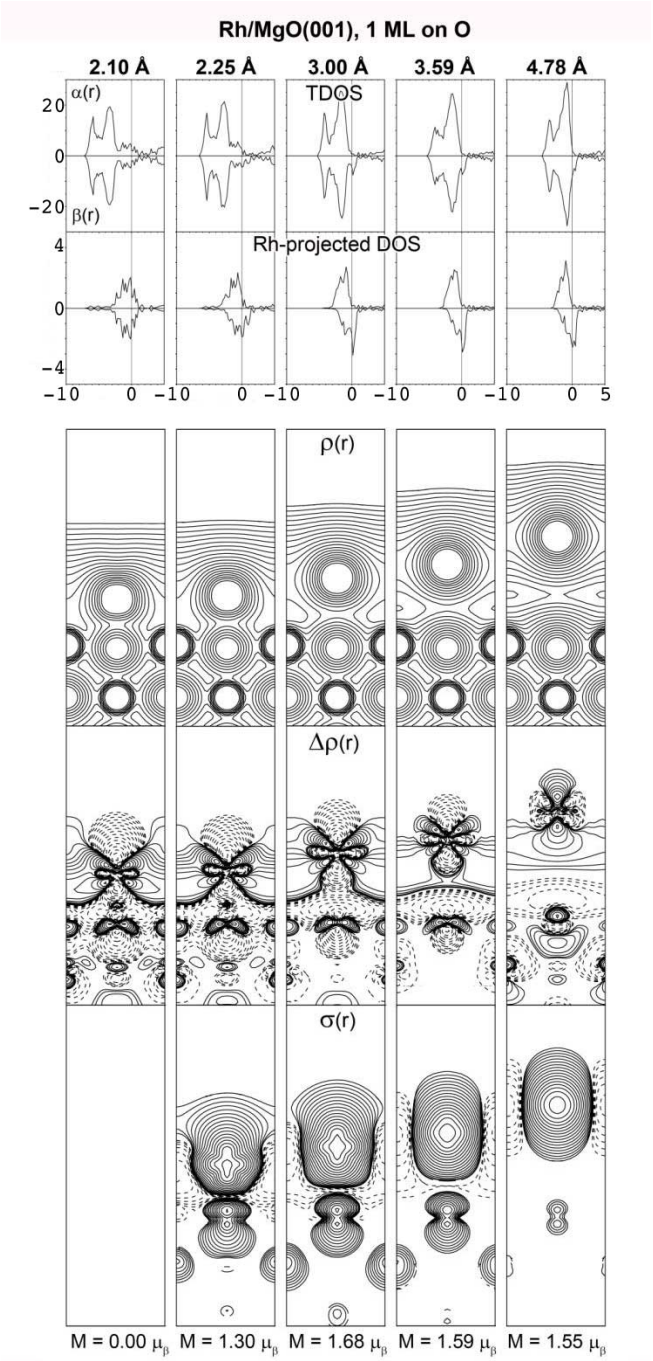
Rh/MgO(001), 1 ML on O
2.10 Å
2.25 Å
3.00 Å
3.59 Å
4.78 Å
α(r)
β(r)
TDOS
Rh-projected DOS
ρ(r)
Δρ(r)
σ(r)
M = 0.00 μβ
M = 1.30 μβ
M = 1.68 μβ
M = 1.59 μβ
M = 1.55 μβ

Fig 5

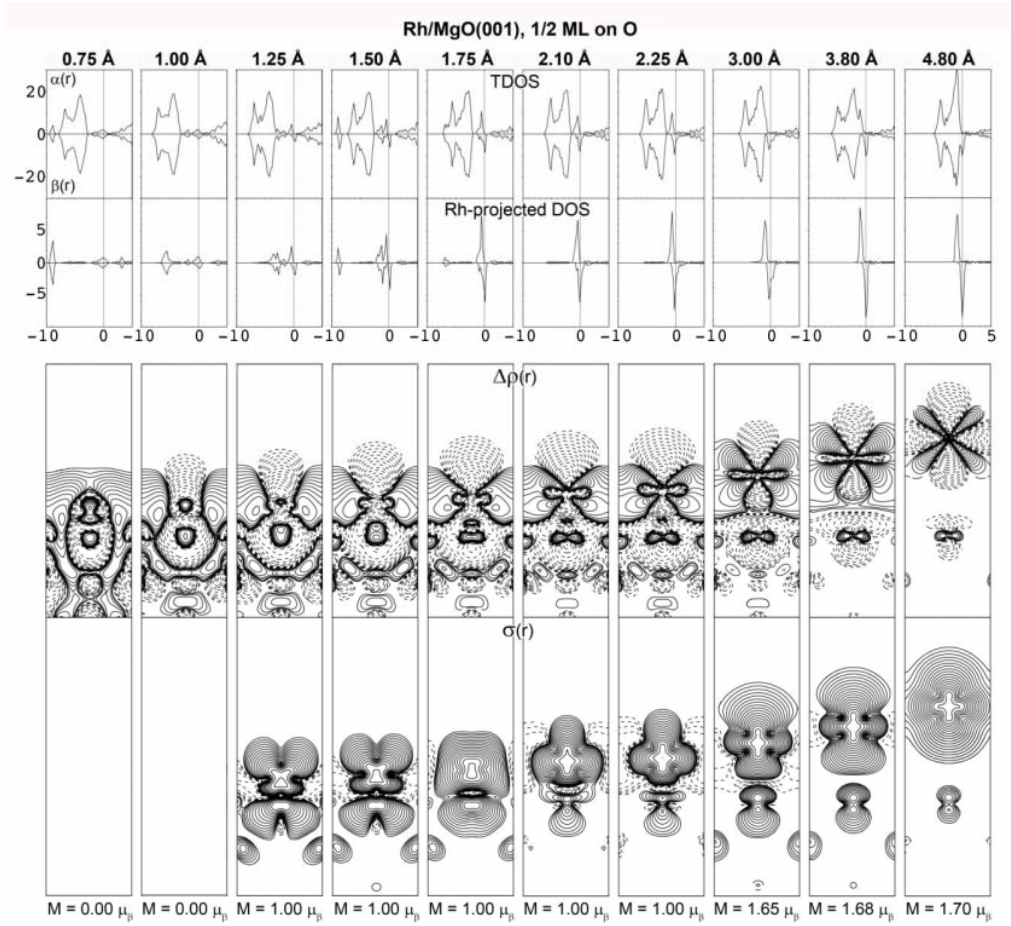
Rh/MgO(001), 1/2 ML on O
0.75 Å
1.00 Å
1.25 Å
1.50 Å
1.75 Å
2.10 Å
2.25 Å
3.00 Å
3.80 Å
4.80 Å
α(r)
β(r)
TDOS
Rh-projected DOS
Δρ(r)
σ(r)
M = 0.00 μβ
M = 0.00 μβ
M = 1.00 μβ
M = 1.00 μβ
M = 1.00 μβ
M = 1.00 μβ
M = 1.00 μβ
M = 1.65 μβ
M = 1.68 μβ
M = 1.70 μβ

Fig 6

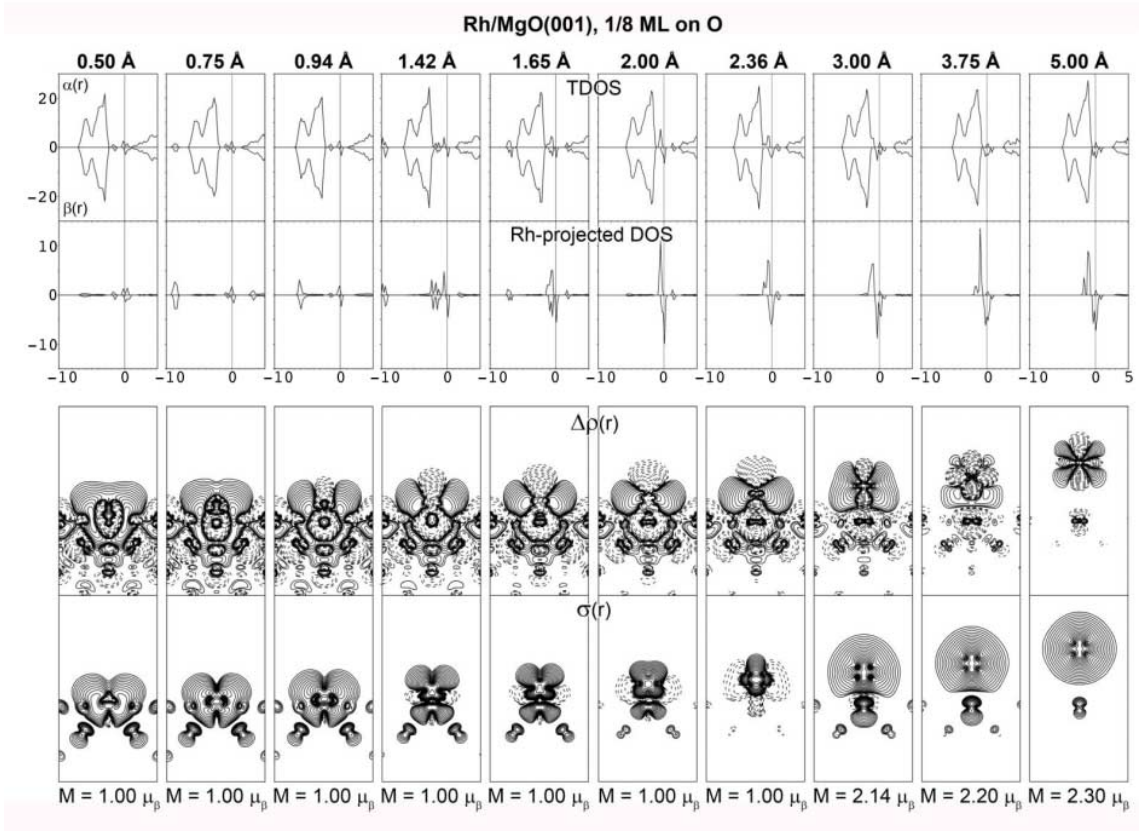
Rh/MgO(001), 1/8 ML on O
0.50 Å
0.75 Å
0.94 Å
1.42 Å
1.65 Å
2.00 Å
2.36 Å
3.00 Å
3.75 Å
5.00 Å
α(r)
β(r)
TDOS
Rh-projected DOS
Δρ(r)
σ(r)
M = 1.00 μβ
M = 1.00 μβ
M = 1.00 μβ
M = 1.00 μβ
M = 1.00 μβ
M = 1.00 μβ
M = 1.00 μβ
M = 2.14 μβ
M = 2.20 μβ
M = 2.30 μβ

Fig 7

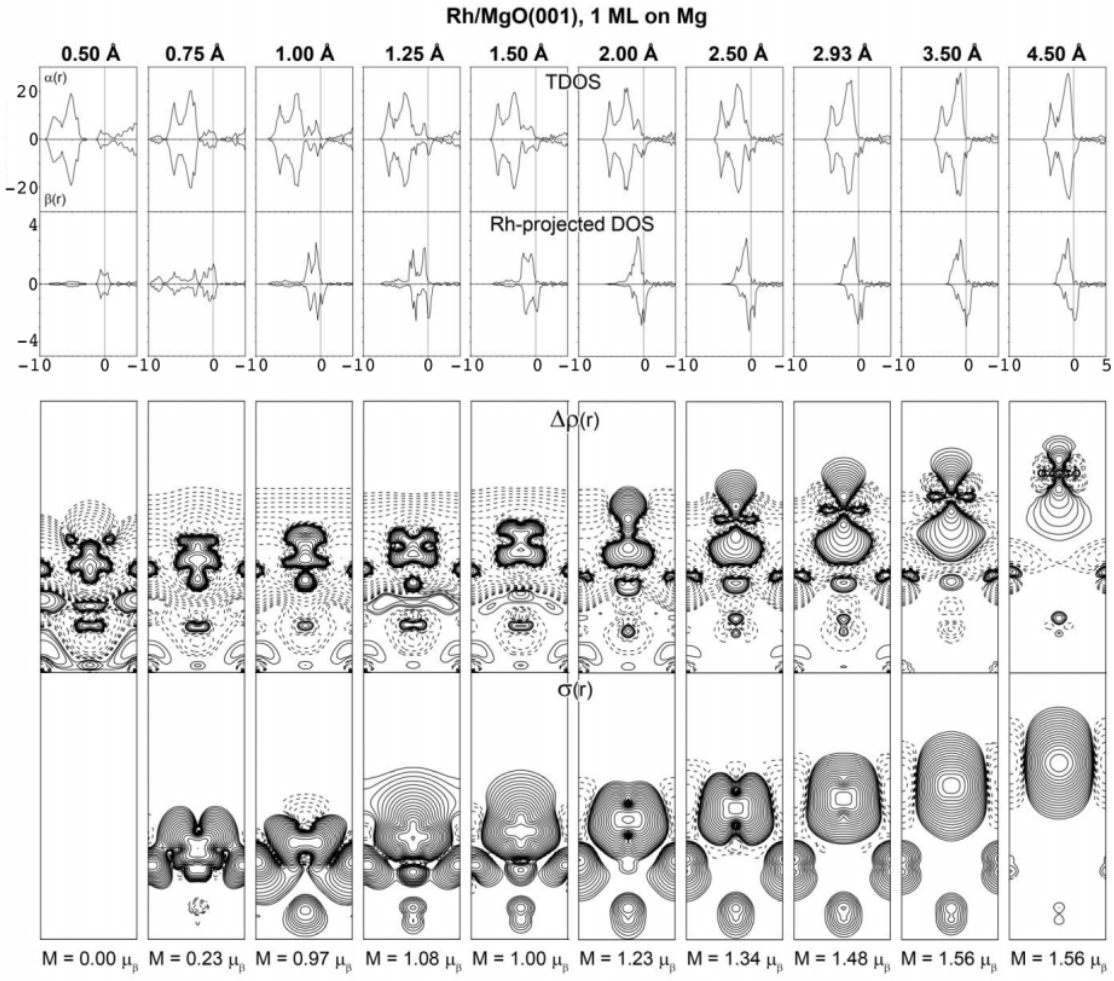
Rh/MgO(001), 1 ML on Mg
0.50 Å
0.75 Å
1.00 Å
1.25 Å
1.50 Å
2.00 Å
2.50 Å
2.93 Å
3.50 Å
4.50 Å
α(r)
β(r)
TDOS
Rh-projected DOS
Δρ(r)
σ(r)
M = 0.00 μβ
M = 0.23 μβ
M = 0.97 μβ
M = 1.08 μβ
M = 1.00 μβ
M = 1.23 μβ
M = 1.34 μβ
M = 1.48 μβ
M = 1.56 μβ
M = 1.56 μβ

Fig 8

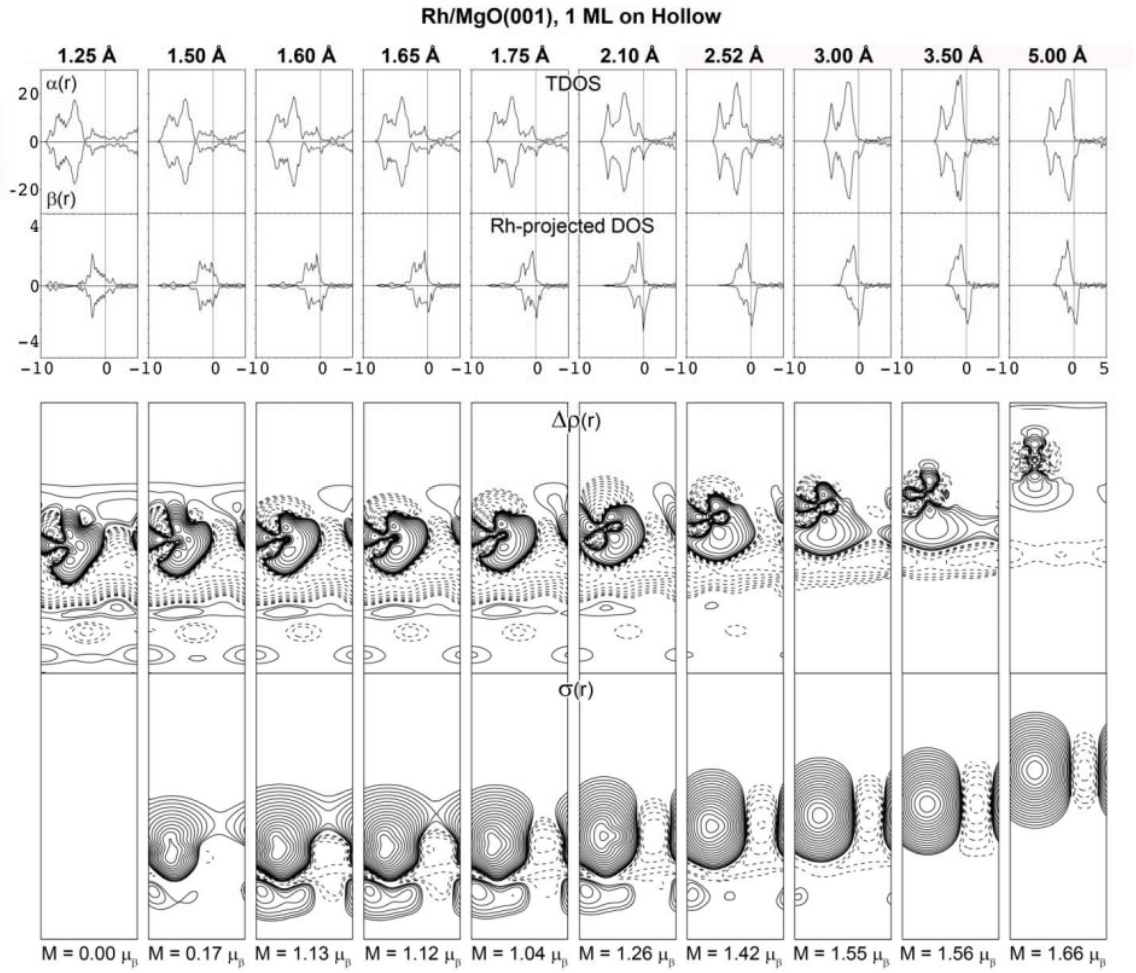
Rh/MgO(001), 1 ML on Hollow
1.25 Å
1.50 Å
1.60 Å
1.65 Å
1.75 Å
2.10 Å
2.52 Å
3.00 Å
3.50 Å
5.00 Å
α(r)
β(r)
TDOS
Rh-projected DOS
Δρ(r)
σ(r)
M = 0.00 μB
M = 0.17 μB
M = 1.13 μB
M = 1.12 μB
M = 1.04 μB
M = 1.26 μB
M = 1.42 μB
M = 1.55 μB
M = 1.56 μB
M = 1.66 μB

Fig 9

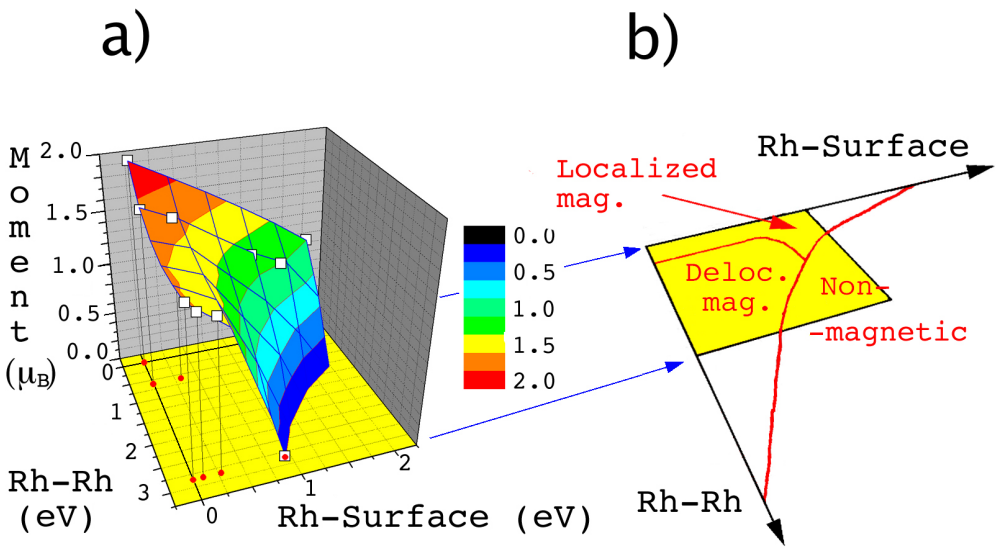
a)
b)
Moment (μ_B)
2.0
1.5
1.0
0.5
0.0
Rh-Rh (eV)
Rh-Surface (eV)
0
1
2
3
0.0
0.5
1.0
1.5
2.0
Localized mag.
Deloc. mag.
Non-magnetic
Rh-Surface
Rh-Rh

Fig 10